

Celastrol regulates bone marrow mesenchymal stem cell fate and bone-fat balance in osteoporosis and skeletal aging by inducing PGC-1 α signaling

Li Li¹, Bing Wang¹, Yawei Li¹, Lei Li¹, Yuliang Dai¹, Guohua Lv¹, Pengfei Wu², Pengzhi Li¹

¹Department of Spine Surgery, The Second Xiangya Hospital, Central South University, Changsha 410011, Hunan, China

²Center for Medical Genetics, School of Life Sciences, Central South University, Changsha 410011, Hunan, China

Correspondence to: Bing Wang; email: wboxyeyy@csu.edu.cn

Keywords: osteoporosis, Celastrol, BM-MSCs, PGC-1 α

Received: August 18, 2019

Accepted: June 13, 2020

Published: July 28, 2020

Copyright: Li et al. This is an open-access article distributed under the terms of the Creative Commons Attribution License (CC BY 3.0), which permits unrestricted use, distribution, and reproduction in any medium, provided the original author and source are credited.

ABSTRACT

Celastrol has recently been identified as a prospective new treatment for obesity and several metabolic complications. However, the effect of Celastrol in osteoporosis (OP) remains unknown. In this study, we demonstrated that Celastrol promotes osteoblast differentiation and prevents adipocyte differentiation in bone marrow mesenchymal stem cells (BM-MSCs) *in vitro*. Mechanistically, Celastrol was able to control the differentiation of BM-MSCs by stimulating PGC-1 α signaling. Moreover, administration of Celastrol could alleviate bone loss and bone marrow adipose tissue (MAT) accumulation in ovariectomized (OVX) mice and aged mice. Together, these results recommended that Celastrol could regulate BM-MSCs fate and bone-fat balance in OP and skeletal aging by stimulating PGC-1 α , which might act as a possible therapeutic target for OP and for the prevention of skeletal aging.

INTRODUCTION

As a common metabolic bone disease, osteoporosis (OP) has become a tremendous public health burden on society. Along with existing patterns of OP caused by imbalances between osteoclasts and osteoblasts, recent evidence has suggested that increased accumulation of bone marrow adipose tissue (MAT) occurred at the expense of bone development, which in turn suppressed osteogenic rejuvenation and hematopoiesis [1–4]. Aging or senescent bone marrow mesenchymal stem cells (BM-MSCs) may show a superior tendency of moving toward adipocytes more than osteoblasts [3]. Although, these molecular mechanisms have been fully identified, only a few drugs have been identified for the treatment of osteoporosis, while outcomes produced by these drugs are not satisfactory and are often accompanied by serious side effects. Therefore, it is essential to identify potential therapeutic targets for osteoporosis.

Celastrol is an active ingredient isolated from the outside covering of the root of the conventional Chinese medicinal plant, thunder god vine [5], and has been shown to exert anti-tumor [6], anti-viral [7], antioxidant stress [8], anti-inflammation [9], immunosuppressive [10] and other activities. Previous reports have shown that Celastrol has been extensively utilized to treat rheumatoid arthritis [11], chronic obstructive pulmonary disease [12], systemic lupus erythematosus [13], obesity [14], insulin resistance [15] and nonalcoholic fatty liver disease (NAFLD) [16]. However, the effects of Celastrol on osteoporosis remain undefined.

In this study, we found that Celastrol could regulate BM-MSCs fate and bone-fat balance in OP and skeletal aging by inducing PGC-1 α , thereby expanding the spectrum of traditional OP treatment methods available in both experimental and clinical settings.

RESULTS

Celastrol promoted the osteogenic differentiation of BM-MSCs *in vitro*

In recent years, research on Celastrol has become increasingly popular due to the therapeutic effects of this active ingredient. In order to investigate the impacts of various dosages of Celastrol on the osteogenic differentiation of BM-MSCs, first a Cell Counting Kit-8 (CCK-8) assay was performed to evaluate the cytotoxicity of Celastrol. The result of CCK-8 assay recommended that Celastrol did not influence cell viability at concentrations of 0.25, 0.5 and 1.0 μM (Figure 1A, $P=0.8264$). Next, the BM-MSCs were cultured in an osteogenesis induction medium with different concentrations of Celastrol. The osteogenic differentiation capacity of BM-MSCs increased in a dosage-dependent manner, as demonstrated using Alizarin Red staining (Figure 1B, 1C, $P<0.0001$ (Figure 1C)). Moreover, osteoblast differentiation markers, alkaline phosphatase (ALP) activity and bone gamma-carboxyglutamic acid-containing protein (BGLAP) secretion also increased, compared with that of control cells (Figure 1D, 1E; $P<0.0001$ (Figure 1D), $P<0.0001$ (Figure 1E)). Moreover, mRNA levels of the osteoblast transcription factors, Osterix and Runx2, were rapidly elevated due to Celastrol treatment in a dosage-dependent manner (Figure 1F, $P<0.0001$). Together, these results recommended that Celastrol induced the osteogenic differentiation of BM-MSCs *in vitro*.

Celastrol inhibited the adipogenic differentiation of BM-MSCs *in vitro*

In order to investigate the impact of different concentrations of Celastrol on the adipogenic differentiation of BM-MSCs, the cells were cultured in an adipogenic induction medium supplied with different concentrations of Celastrol. The adipogenic differentiation capacity of BM-MSCs diminished in a dosage-dependent manner, as demonstrated using oil red staining (Figure 2A, 2B; $P<0.0001$ (Figure 2B)). Furthermore, the mRNA levels of peroxisome proliferator-activated receptor-g (Pparg) and fatty acid binding protein 4 (Fabp4), two main indicators of adipocyte differentiation, also decreased (Figure 2C, $P<0.0001$). Together, these results recommended that Celastrol inhibited the adipogenic differentiation of BM-MSCs *in vitro*.

Celastrol regulated the differentiation of BM-MSCs by activating PGC-1 α signaling

Accumulation of oxidative stress is related to bone loss in OP and skeletal aging [17, 18]. PGC-1 α plays an

important role in regulating oxidative stress in multifarious mitochondria-rich tissues [19, 20]. More importantly, PGC-1 α can reduce ROS in BM-MSCs, participating in controlling lineage decisions between osteoblasts and adipocytes fate of BM-MSCs [21]. We established that the transcript levels of PGC-1 α mRNA in BM-MSCs treated with Celastrol were obviously elevated (Figure 3A, $P<0.0001$). Furthermore, levels of UCP2 and Catalase, which are negative regulators of ROS, were also significantly elevated (Figure 3A, $P<0.0001$). Western blotting analysis further confirmed that Celastrol could promote the protein expression levels of PGC-1 α (Figure 3B). Moreover, the acetylation levels of PGC1 α decreased in the Celastrol-treated group (Figure 3C).

In order to identify pathways involved in activating PGC-1 α by Celastrol, we measured the rate of phosphorylation of AMP kinase (AMPK) and expression of SIRT1 in BM-MSCs using western blotting analysis. The results revealed that the Celastrol-treated group showed significantly higher levels of AMPK activity (exhibited as pAMPK/AMPK, $P=0.0003$) and higher levels of SIRT1, compared with the control group (Figure 3D, 3E). In order to confirm whether Celastrol regulated the fate of BM-MSCs via activation of PGC-1 α signaling, we silenced PGC-1 α signaling in BM-MSCs using siRNAs and then treated BM-MSCs with Celastrol. The successful establishment of the inhibition of PGC-1 α in BM-MSCs was confirmed using western blotting analysis (Figure 3F). Interestingly, Celastrol supplementation could enhance osteogenic differentiation and abrogate adipogenic differentiation in BM-MSCs of the WT control group (Figure 3G–3J; $P<0.0001$ (Figure 3H, left panel), $P<0.0001$ (Figure 3J, left panel)). Nevertheless, in the PGC-1 α -knockdown group, Celastrol failed to restore homeostasis between osteogenic and adipogenic differentiation of BM-MSCs (Figure 3G–3J; $P=0.5283$ (Figure 3H, right panel), $P=0.0582$ (Figure 3J, right panel)).

In order to further confirm the role of PGC-1 α *in vivo*, PGC-1 α -knockout (PGC-1 $\alpha^{-/-}$) mice (2 month old) and WT mice (2 month old) were ovariectomized. 12 weeks later, the mice were intraperitoneally injected with Celastrol (200 $\mu\text{g}/\text{kg}$) or DMSO (control), every two days for 4 weeks. As expected, Celastrol treatment reduced the number and area of adipocytes in the bone marrow and increased the number and surface of osteoblasts on trabecular and endosteal bone surfaces in WT OVX mice, while the curative effect of Celastrol in PGC-1 $\alpha^{-/-}$ OVX mice was offset (Figure 3K). Taken together, these results indicated that Celastrol regulated the differentiation of BM-MSCs by activating PGC-1 α signaling.

Administration of Celastrol alleviated bone loss and MAT accumulation in aged mice

In order to explore the remedial potential of Celastrol on aging-associated osteoporosis, aged (18 month old) male mice were intraperitoneally injected with Celastrol

(200 µg/kg, 98% (HPLC), Sigma, St. Louis, MO) or DMSO (control) every two days for 4 weeks. Mice treated with Celastrol showed increased PGC-1 α expression levels, compared with the vehicle-treated group (Figure 4A, $P=0.0003$). As a result, Celastrol augmented trabecular bone volume and number, as well

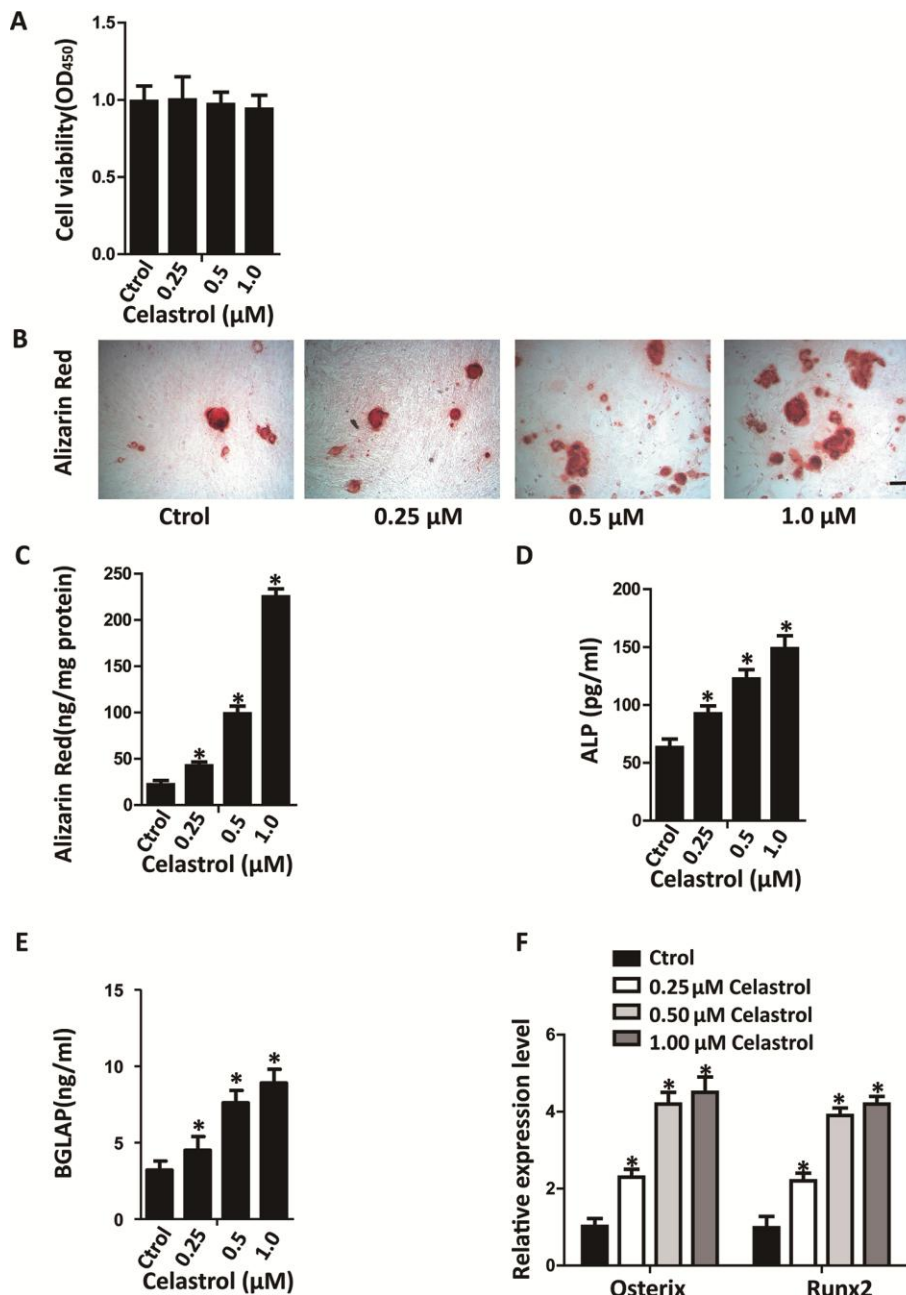


Figure 1. Celastrol promoted the osteogenic differentiation of BM-MSCs *in vitro*. (A) BM-MSCs were seeded into 96-well plates at a density of 8×10^3 cells/well and treated with different concentrations of Celastrol for 48 h. Cell viability was determined using CCK-8 assay. (B, C) Representative images of Alizarin Red S staining (B) and quantitative analysis (C) of matrix mineralization of BM-MSCs cultured in the osteogenesis induction medium for 21 days. Scale bar: 100 µm. (D, E) Analysis of ALP activity (D) and osteocalcin secretion (E) of BM-MSCs cultured in the osteogenesis induction medium for 48 hours ($n = 3$ per group). (F) qRT-PCR analysis of the relative levels of Osterix and Runx2 mRNA expression in BM-MSCs cultured in the osteogenesis induction medium for 48 hours ($n = 3$ per group). Results are shown as mean \pm SD. Statistical significance was determined using analysis of variance (one-way ANOVA). * $P < 0.0001$ compared with control.

as cortical bone thickness, and reduced trabecular separation and the endosteal perimeter (Figure 4B–4G; $P=0.0031$ (Figure 4C), $P=0.0084$ (Figure 4D), $P=0.0187$ (Figure 4E), $P=0.0263$ (Figure 4F), $P=0.0259$ (Figure 4G)). Moreover, the bone strength of Celastrol treated mice was higher (Figure 4H–4I; $P=0.0021$ (Figure 4H), $P=0.0031$ (Figure 4I)). Vertebral bone volume was also higher in Celastrol treated mice, compared with the vehicle-treated group (Figure 4J–4K; $P<0.0001$ (Figure 4K)). In addition, Celastrol-treated mice showed an obviously lower number and area of adipocytes in bone marrow and a higher number and surface area of osteoblasts on the trabecular and endosteal bone surfaces (Figure 4L). Thus, together these results indicated that the administration of Celastrol alleviated bone loss and MAT accumulation in aged mice.

Celastrol treatment increased bone formation and decreased bone marrow fat in OVX mice

Ovariectomy (OVX) is a well-known model utilized to trigger postmenopausal estrogen deficiency as well as prompt osteoporotic bone loss. In order to further confirm the therapeutic effect of Celastrol, OVX mice

were intraperitoneally injected with Celastrol, as mentioned above. Similar to the results obtained from the previous experiment, mice treated with Celastrol showed elevated PGC-1 α expression levels (Figure 5A, $P=0.0008$). Furthermore μ CT analysis indicated that mice treated with Celastrol showed a significantly greater increase in trabecular bone volume, number as well as cortical thickness, and a reduction in trabecular separation and endosteal perimeter (Figure 5B–5G; $P=0.0054$ (Figure 5C), $P < 0.0001$ (Figure 5D), $P=0.0167$ (Figure 5E), $P=0.0004$ (Figure 5F), $P < 0.0001$ (Figure 5G)). Furthermore, bone strength was greater in the Celastrol treated group (Figure 5H–5I; $P<0.0001$ (Figure 5H), $P < 0.0001$ (Figure 5I)). Furthermore, the vertebral bone volume of Celastrol treated mice had increased (Figure 5J–5K; $P < 0.0001$ (Figure 5K)). Meanwhile, adipocyte numbers along with the area of bone marrow covered by them had significantly decreased and the number and surface of osteoblasts on trabecular and endosteal bone surfaces had increased in Celastrol treated mice (Figure 5L). These outcomes recommended that Celastrol treatment increased bone formation and decreased bone marrow fat in OVX mice.

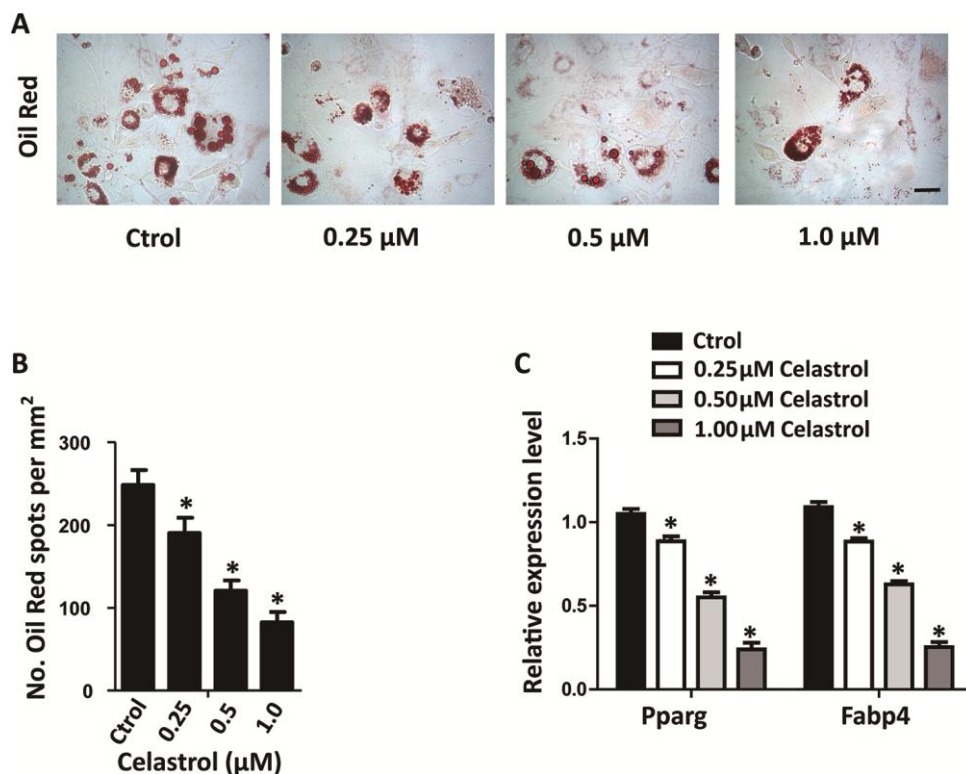


Figure 2. Celastrol inhibited the adipogenic differentiation of BM-MSCs *in vitro*. (A, B) Representative images of Oil Red O staining of lipids (A) and quantification of the number of spots (B) on BM-MSCs cultured in the adipogenesis induction medium for 14 days. Scale bar: 100 μ m. (C) qRT-PCR analysis of the relative levels of Pparg and Fabp4 mRNA expression in BM-MSCs cultured in the adipogenesis induction medium for 48 hours ($n = 3$ per group). Results are shown as mean \pm SD. Statistical significance was determined using analysis of variance (one-way ANOVA). * $P < 0.0001$ compared with control.

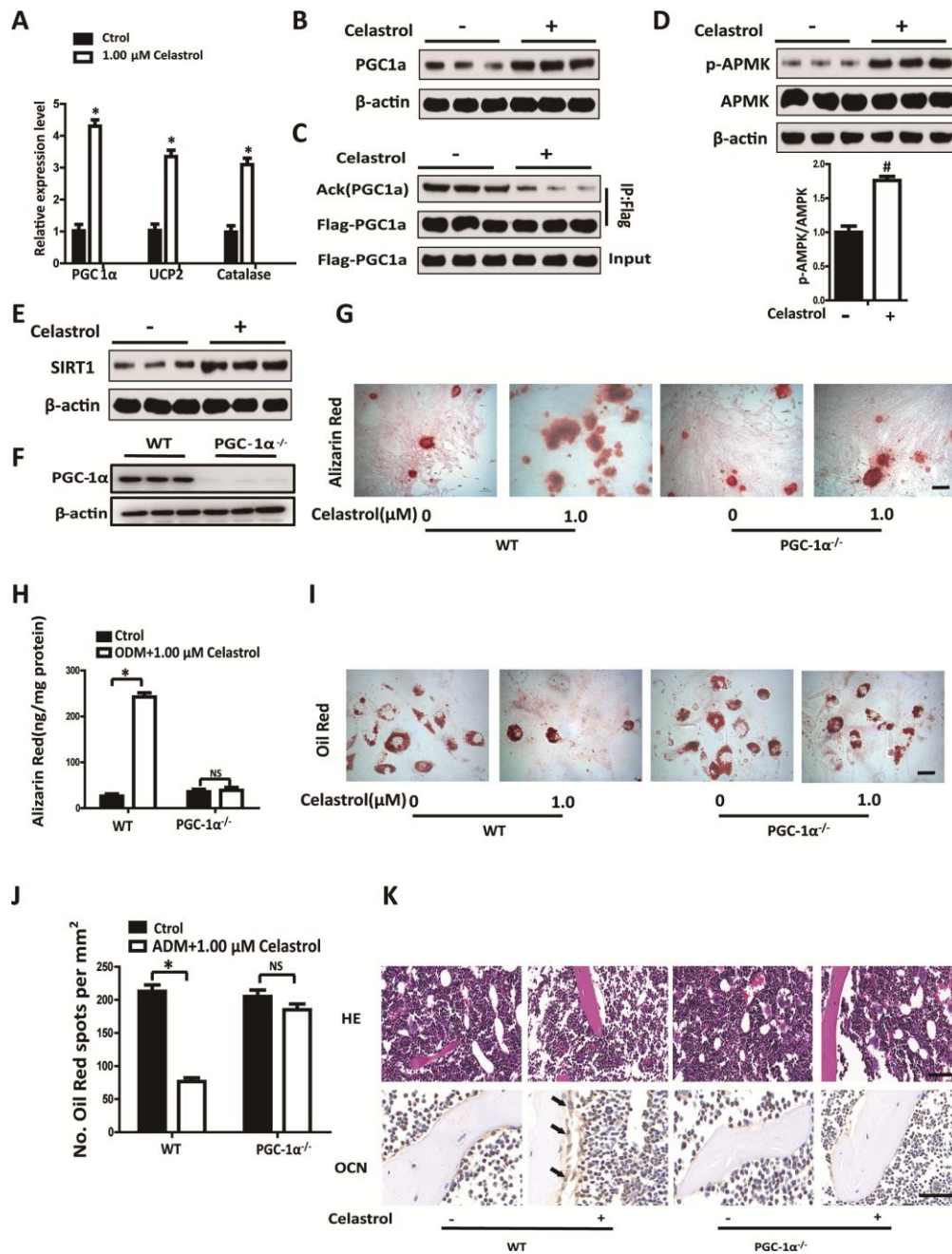


Figure 3. Celastrol regulated the differentiation of BM-MSCs by activating PGC-1 α signaling. (A) Expression levels of PGC-1 α , UCP2 and Catalase in BM-MSCs treated with the vehicle or Celastrol (1.0 μ M, 48 hours) ($n = 3$ per group). (B) Western blotting analysis of the protein levels of PGC-1 α of BM-MSCs treated with the vehicle or Celastrol (1.0 μ M, 48 hours). (C) Western blotting analysis for the detection of PGC1 α acetylation levels in PGC1 α immunoprecipitates obtained from BM-MSCs transfected with pcDNA-Flag-PGC1 α and treated with the vehicle or Celastrol (1.0 μ M, 48 hours). (D) Western blotting analysis for the detection of pAMPK in BM-MSCs treated with the vehicle or Celastrol (1.0 μ M, 48 hours). The levels of pAMPK were quantified using ImageJ software and were normalized to total AMPK levels (D, bottom). (E) Western blotting analysis of the protein levels of SIRT-1 in BM-MSCs treated with the vehicle or Celastrol (1.0 μ M, 48 hours). (F) Western blotting analysis of the relative levels of PGC-1 α in BM-MSCs transfected with PGC-1 α siRNA. (G, H) Representative images of Alizarin Red staining (G) and quantitative analysis (H) of matrix mineralization of BM-MSCs cultured in the osteogenesis induction medium for 21 days. Scale bar: 100 μ m. (I, J) Representative images of Oil Red O staining of lipids (I) and quantification of the number of spots (J) on BM-MSCs cultured in the adipogenesis induction medium for 14 days. Scale bar: 100 μ m. (K) PGC-1 α -knockout (PGC-1 α ^{-/-}) mice (2 month old) and WT mice (2 month old) were ovariectomized. 12 weeks later, they were intraperitoneally injected with Celastrol (200 μ g/kg) or DMSO (control) every two days for 4 weeks. H&E staining (top) and osteocalcin immunohistochemical staining (bottom) of the bone were conducted to evaluate the numbers and area covered by adipocytes and osteoblasts after Celastrol treatment. Scale bar: 100 μ m. Data are presented as mean \pm SD. Statistical significance was determined using the *t*-test. * $P < 0.0001$; # $P < 0.001$ compared with control.

DISCUSSION

The occurrence of OP along with its complications are rapidly increasing globally. Therefore, it is imperative to identify more effective and safer therapy options for osteoporosis. Previous scientific evidence has found

that BM-MSCs have a tendency to differentiate into adipocytes rather than osteoblasts as age increases, resulting in the gradual accumulation of fat and bone loss [22]. Thus, BM-MSCs are regarded as promising therapeutic targets for OP. In this study, our results demonstrated that Celastrol promotes osteoblast

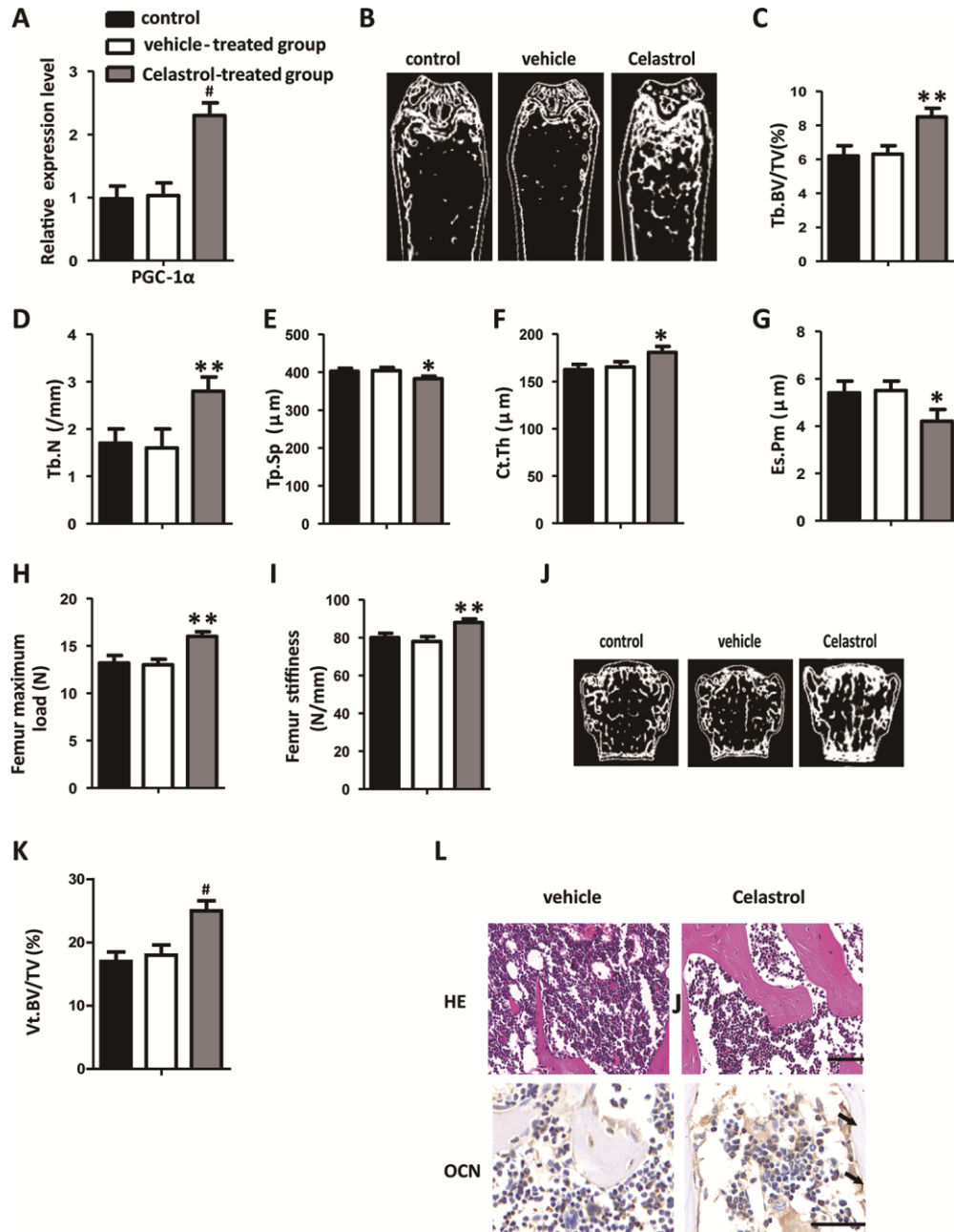


Figure 4. Administration of Celastrol alleviated bone loss and MAT accumulation in aged mice. (A) mRNA expression level of PGC-1 α in the BM-MSCs determined using qRT-PCR (n = 3 per group). (B–G) Representative μ CT images (B) and quantitative μ CT analysis of trabecular (C–E) and cortical (F, G) bone microarchitecture in the femora of Celastrol-treated mice. n = 6–7 per group. (H–I) Three-point bending measurement of femur maximum load (H) and stiffness (I). n = 5 per group. (J, K) Representative μ CT images (J) and quantification of the ratio of bone volume to tissue volume (K) of L4 vertebrae (Vt. BV/TV). n = 6 per group. (L) Representative images of H&E staining (L, top) and osteocalcin immunohistochemical staining (L, bottom). Scale bars: 100 μ m. n = 5 per group. Data are presented as mean \pm SD. Statistical significance was determined using analysis of variance (one-way ANOVA). [#] $P < 0.001$; ^{**} $P < 0.01$; ^{*} $P < 0.05$.

differentiation as well as inhibits adipocyte differentiation in BM-MSCs *in vitro*. Consistent with our results, Hong's research also found that Celastrol exerted an inhibitory effect on lipid accumulation and the adipogenesis of human adipose-derived stem cells (hADSCs) [23]. Additionally, Celastrol could regulate the function of bone marrow-derived endothelial progenitor cells (BM-EPCs) [24].

More importantly, we found that Celastrol controlled the differentiation of BM-MSCs by inducing PGC-1 α signaling. Reactive oxygen species (ROS)-induced oxidative stress rises along with aging, resulting in the pathophysiology of aging related OP and postmenopausal osteoporosis [25, 26]. Excessive levels of ROS can prevent the differentiation and development of osteoblasts [27]. PGC-1 α performs an imperative function in

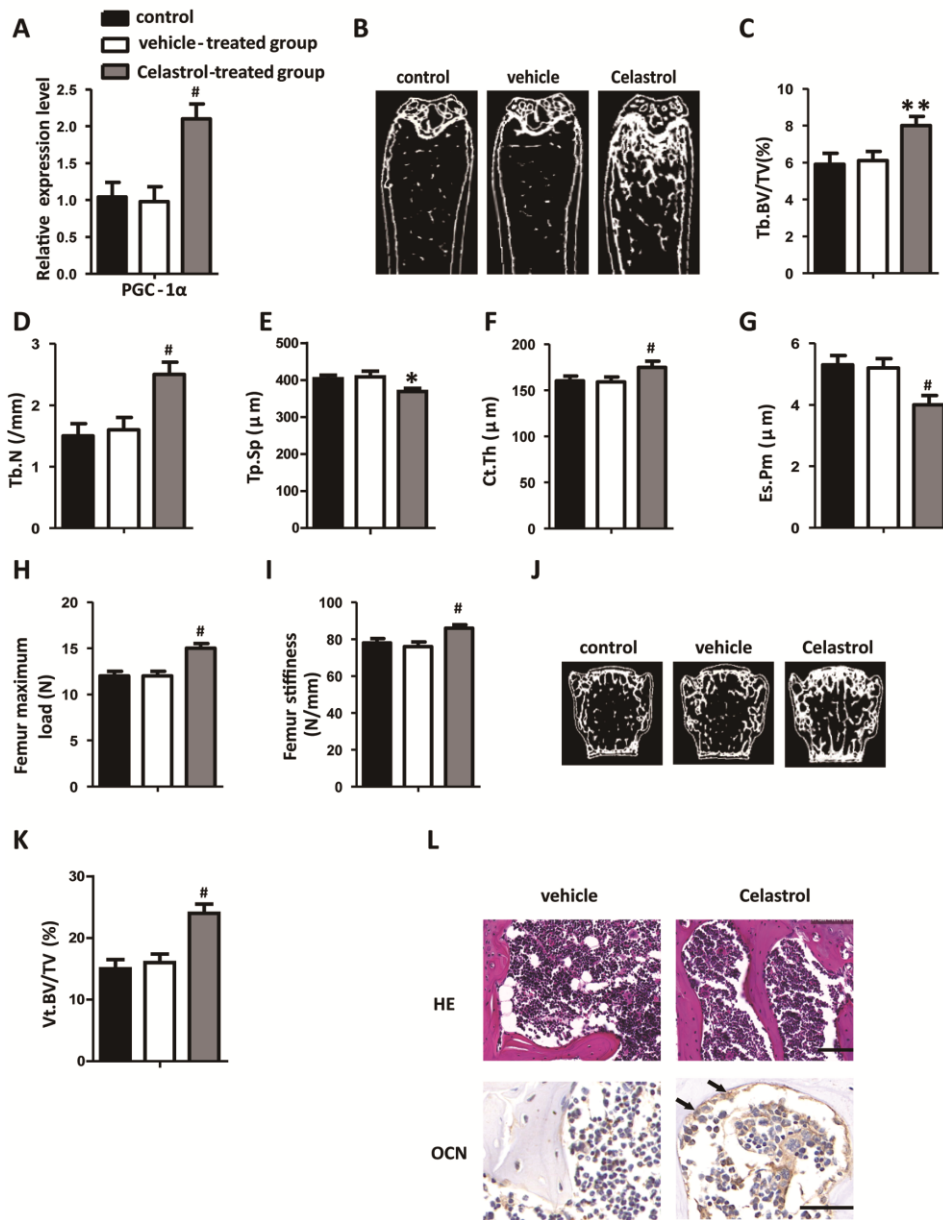


Figure 5. Celastrol treatment increased bone formation and reduced bone marrow fat in OVX mice. (A) mRNA expression level of PGC-1 α in the BM-MSCs determined using qRT-PCR (n = 3 per group). (B–G) Representative μ CT images (B) and quantitative μ CT analysis of trabecular (C–E) and cortical (F, G) bone microarchitecture of the femora of Celastrol-treated mice. n = 6-7 per group. (H–I) Three-point bending measurement of femur maximum load (H) and stiffness (I). n = 5 per group. (J, K) Representative μ CT images (J) and quantification of the ratio of bone volume to tissue volume (K) of L4 vertebrae (n = 6 per group). (L) Representative images of H&E staining (L, top) and osteocalcin immunohistochemical staining (L, bottom). Scale bars: 100 μ m. n = 5 per group. Data are presented as mean \pm SD. Statistical significance was determined using analysis of variance (one-way ANOVA). # P < 0.001; ** P < 0.01, * P < 0.05.

defending against ROS produced by mitochondrial activity via its capability to stimulate several antioxidant enzymes, including SOD, catalase and glutathione peroxidases [28]. The results of Yu's research study indicated that PGC-1 α is critically involved in determining the fate of BM-MSCs as well as the prevention of MAT buildup as a result of OP and skeletal aging [21]. In our study, we found that mRNA and protein expression level of PGC-1 α in BM-MSCs treated with Celastrol were obviously elevated. Furthermore, levels of UCP2 and Catalase, which are negative regulators of ROS, also significantly increased. Likewise, other reports also found that Celastrol could augment PGC-1 α expression in adipocytes and skeletal muscles [29, 30].

AMPK and SIRT1 are major upstream regulators of PGC-1 α and are inhibited in pathological conditions such as oxidative stress and aging [31]. The activation of AMPK and SIRT1 produces beneficial effects on these conditions. In NAFLD mice, Celastrol could enhance the phosphorylation of AMPK and induce hepatic SIRT1 expression [16]. Consistently, our results revealed that Celastrol could increase AMPK phosphorylation and SIRT1 protein expression levels. Taken together, our data recommended that Celastrol regulated the differentiation of BM-MSCs by activating the AMPK/SIRT1-PGC-1 α signaling pathway. Similarly, Wang's study also found that Celastrol could exert an anti-inflammatory effect in liver fibrosis by increasing AMPK- PGC-1 α signaling [32]. In diabetic rats, Celastrol was found to have exerted antioxidant effects on the skeletal muscle, partially by regulating the AMPK-PGC1 α -Sirt3 signaling pathway [30].

Celastrol is a traditional Chinese medicine that exerts many biological activities. Celastrol could attenuate intrahepatic cholestasis in pregnancy by preventing matrix Metalloproteinases-2 and -9 [33]. Ma et al. found that Celastrol exerted protective effects against obesity and metabolic dysfunction via stimulation of the HSF1/PGC1 α transcriptional axis [34]. It has been documented that Celastrol-induced the prevention of NF- κ B scheme associates by exerting an anti-inflammatory response [35, 36] and anti-cancer effect [37]. Furthermore, Celastrol could ameliorate acetaminophen-induced oxidative stress as well as cytotoxicity in HepG2 cells [38]. However, only a few studies have been conducted on the therapeutic effect of Celastrol on osteoporosis. In this study, we established that the administration of Celastrol could alleviate bone loss and MAT accumulation in old mice and OVX mice.

These outcomes indicated that Celastrol could regulate bone marrow stem cell differentiation and bone-fat

balance in OP and skeletal aging by stimulating PGC-1 α , which might act as a possible therapeutic target for OP and for the prevention of skeletal aging.

MATERIALS AND METHODS

Cell culture

Mice BM-MSCs were acquired and cultured, as described in previous reports [39, 40]. In brief, bone marrow cells acquired from the bone marrow cavity of 8 week old mice were incubated at 4°C for 20 min along with the following antibodies: Sca-1, CD29, CD45 and CD11b. Thereafter, Sca-1⁺CD29⁺CD45⁻CD11b⁻ BM-MSCs were separated using flow cytometry (BD Biosciences) and cultured in DMEN supplemented with 10% FBS (Gibco, Invitrogen, USA) and 1% penicillin/streptomycin.

For the transfection of PGC-1 α siRNA and its respective negative control (NC), the BM-MSCs were seeded into 12-well plates and transfected on a lipofectamine 2000 system (Thermo Scientific), according to manufacturer's recommendations.

Cell viability

We used CCK-8 assay to assess the viability of BM-MSCs after Celastrol treatment, as instructed by the supplier. Absorbance was measured at 450 nm via a microplate reader (Thermo Electron Corp).

Animals

Pathogen free (SPF) C57BL/6J mice were obtained from Hunan SLACCAS Jingda Experimental Animal Co. Ltd., while PGC-1 α ^{-/-} mice were obtained from Jackson Laboratories. All animals were housed under 12-hour light/dark cycles and were provided unrestricted access to food and water, unless otherwise specified. This study was approved by the Animal Care Committee of Central South University.

For prior to ovarian surgery, OVX mice (2-month-old) were intraperitoneally injected with ketamine (80 mg/kg.bw) plus xylazine (10 mg/kg.bw). Then, the mice were kept in the lateral position and the dorsal and ventral skin was disinfected with a cotton soaked in alcohol. An incision of about 5 mm in length was made on the area ventral to the erector spinae caudal from the last rib through ophthalmology. The lower lumbar muscle was cut to locate the ovaries, which was surrounded by adipose tissue. Both sides of each ovary were ligated and the ovaries were removed. Once the surgery was completed, the incision was sutured, and the mice were placed in warm cages for recovery.

Table 1. Primer sequences used for real-time PCR analysis.

Gene	Forward primer	Reverse primer
Actin(mouse)	GGCTGTATTCCCTCCATCG	CCAGTTGGTAACAATGCCATGT
Actin(human)	CGTGGACATCCGCAAAGA	TCGTCATACTCCTGCTTGCTG
Runx2 (mouse)	ACTTCCTGTGCTCCGTGCTG	TCGTTGAACCTGGCTACTTGG
Osterix (mouse)	ACCAGGTCCAGGCAACAC	GCAAAGTCAGATGGGTAAGTAG
PPAR α (mouse)	GACCACTCGCATTCCCTT	CCACAGACTCGGCACTCA
Fabp4 (mouse)	AAATCACC GCAGACGACA	CACATTCCACCACCAGCT
PGC-1 α (mouse)	AGCCGTGACCACTGACAACGAG	GCTGCATGGTTCTGAGTGCTAAG
PGC-1 α (human)	TCTGAGTCTGTATGGAGTGACAT	CCAAGTCGTTACATCTAGTTCA
UCP2 (mouse)	ACAAGACCATTGCACGAGAG	ATGAGGTTGGCTTTCAGGAG
Catalase(mouse)	TGAGAAGCCTAAGAACGCAATTC	TGAGAAGCCTAAGAACGCAATTC

Administration of Celastrol

For intraperitoneal (i.p.) treatment, mice received 25 μ l of vehicle (DMSO) on four consecutive days as acclimation before the doses of Celastrol or vehicle treatment indicated were administered. Celastrol was dissolved in DMSO solution and the mice were administered intraperitoneal injections of Celastrol (200 μ g/kg), every two days for 4 weeks. Vehicle groups received the same volume of DMSO for control purposes during the experiments.

Osteogenic differentiation and mineralization assay

In order to induce osteoblastic differentiation, BM-MSCs were cultured in 24-well plates at appropriate densities in an osteogenesis induction medium for 48 hours. Then, the culture media were obtained for evaluation of ALP activity and osteocalcin levels using ELISA kits, as instructed by the supplier.

In order to induce osteoblastic mineralization, the above mentioned process was performed in 6-well plates at appropriate densities with an osteogenesis induction medium for 21 days. Alizarin Red staining was conducted and used to quantitatively assess cell matrix mineralization.

Adipogenic differentiation assay

In order to induce adipogenic differentiation, BM-MSCs were cultured in 6-well plates at a density of 2.5×10^6 cells/well in an adipogenesis induction medium for 14 days. Oil Red O staining was performed to identify mature adipocytes in the culture.

Immunoprecipitation and Western blotting analysis

Cells were transfected with pcDNA-Flag-PGC1 α . After 24–48 hours, the cells were lysed in a lysis buffer with a protease inhibitor cocktail, cleared using centrifugation,

and subjected to immunoprecipitation using Flag-conjugated beads (Sigma-Aldrich). After 2 to 3 hours, the beads were washed, resuspended in a protein loading buffer, and boiled. Then, the supernatant was subjected to SDS-PAGE and proteins were detected using the indicated antibodies.

Immunohistochemical staining

Immunohistochemical staining was conducted, as previously described [41, 42]. Bone segments were treated for antigen recovery through assimilation with 0.05% trypsin at 37°C for 15 minutes, and were then probed using a primary antibody against osteocalcin (Takara) overnight at 4°C. Consequently, an HRP-streptavidin recognition system (Dako) was utilized to distinguish immunoactivity, followed by counterstaining with hematoxylin (Sigma). The segments probed with polyclonal rabbit IgG (R&D Systems Inc.) acted as negative controls.

qRT-PCR analysis

Total RNA was extracted using TRIzol reagent (Thermo Fisher). qPCR was performed using a PrimeScript RT reagent Kit (Takara) and SYBR Green PCR Master Mix (Takara). Each value was adjusted by using β -actin levels as reference. The list of primers used are mentioned in Table 1.

Micro-CT analysis

The femurs were separated from mice and fixed in 4% paraformaldehyde overnight. Next, they were imaged and evaluated using high-resolution micro-CT analysis (Skyscan 1172, Bruker MicroCT). We selected an area of 5% of femoral length below the growth plate for examination. Trabecular bone volume per tissue volume (Tb. BV/TV), trabecular number (Tb.N), trabecular separation (Tb.Sp) and trabecular thickness (Tb.Th) were determined.

Statistical analysis

The results are expressed as mean \pm SD. Two-tailed Student's *t* test (for comparison between two groups) as well as one-way ANOVA (for comparison between multiple groups) were performed. All experiments were repeated a minimum of 3 times. A *P* value of < 0.05 signified statistical significance.

AUTHOR CONTRIBUTIONS

Li Li wrote the first draft of the manuscript. Bing Wang developed the structure and arguments for the paper. Li Li, Yawei Li and Lei Li performed the experiments. Yawei Li, Lei Li, Yuliang Dai, Guohua Lv, Pengfei Wu and Pengzhi Li discussed and edited different parts of the manuscript. All authors read and approved the final manuscript.

CONFLICTS OF INTEREST

The authors declare that they have no competing interests.

FUNDING

This work was supported by a grant from the National Natural Science Foundation of China (No. 81871748).

REFERENCES

1. Devlin MJ, Rosen CJ. The bone-fat interface: basic and clinical implications of marrow adiposity. *Lancet Diabetes Endocrinol.* 2015; 3:141–47. [https://doi.org/10.1016/S2213-8587\(14\)70007-5](https://doi.org/10.1016/S2213-8587(14)70007-5) PMID:24731667
2. Ambrosi TH, Scialdone A, Graja A, Gohlke S, Jank AM, Bocian C, Woelk L, Fan H, Logan DW, Schürmann A, Saraiva LR, Schulz TJ. Adipocyte accumulation in the bone marrow during obesity and aging impairs stem cell-based hematopoietic and bone regeneration. *Cell Stem Cell.* 2017; 20:771–84.e6. <https://doi.org/10.1016/j.stem.2017.02.009> PMID:28330582
3. Fan Y, Hanai JI, Le PT, Bi R, Maridas D, DeMambro V, Figueroa CA, Kir S, Zhou X, Mannstadt M, Baron R, Bronson RT, Horowitz MC, et al. Parathyroid hormone directs bone marrow mesenchymal cell fate. *Cell Metab.* 2017; 25:661–72. <https://doi.org/10.1016/j.cmet.2017.01.001> PMID:28162969
4. Li H, Xie H, Liu W, Hu R, Huang B, Tan YF, Xu K, Sheng ZF, Zhou HD, Wu XP, Luo XH. A novel microRNA targeting HDAC5 regulates osteoblast differentiation in mice and contributes to primary osteoporosis in humans. *J Clin Invest.* 2009; 119:3666–77. <https://doi.org/10.1172/JCI39832> PMID:19920351
5. Ng SW, Chan Y, Chellappan DK, Madheswaran T, Zeeshan F, Chan YL, Collet T, Gupta G, Oliver BG, Wark P, Hansbro N, Hsu A, Hansbro PM, et al. Molecular modulators of celestrol as the keystones for its diverse pharmacological activities. *Biomed Pharmacother.* 2019; 109:1785–92. <https://doi.org/10.1016/j.biopha.2018.11.051> PMID:30551432
6. Jiang Z, Cao Q, Dai G, Wang J, Liu C, Lv L, Pan J. Celestrol inhibits colorectal cancer through TGF- β 1/smad signaling. *Onco Targets Ther.* 2019; 12:509–18. <https://doi.org/10.2147/OTT.S187817> PMID:30666129
7. Kim HR, Lee D, Eom YB. Anti-biofilm and anti-virulence efficacy of celestrol against *Stenotrophomonas maltophilia*. *Int J Med Sci.* 2018; 15:617–27. <https://doi.org/10.7150/ijms.23924> PMID:29725253
8. Gu L, Bai W, Li S, Zhang Y, Han Y, Gu Y, Meng G, Xie L, Wang J, Xiao Y, Shan L, Zhou S, Wei L, et al. Celestrol prevents atherosclerosis via inhibiting LOX-1 and oxidative stress. *PLoS One.* 2013; 8:e65477. <https://doi.org/10.1371/journal.pone.0065477> PMID:23799016
9. Allen SD, Liu YG, Kim T, Bobbala S, Yi S, Zhang X, Choi J, Scott EA. Celestrol-loaded PEG-b-PPS nanocarriers as an anti-inflammatory treatment for atherosclerosis. *Biomater Sci.* 2019; 7:657–68. <https://doi.org/10.1039/c8bm01224e> PMID:30601470
10. Zhang J, Shan J, Chen X, Li S, Long D, Li Y. Celestrol mediates Th17 and treg cell generation via metabolic signaling. *Biochem Biophys Res Commun.* 2018; 497:883–89. <https://doi.org/10.1016/j.bbrc.2018.02.163> PMID:29476742
11. Fang Z, He D, Yu B, Liu F, Zuo J, Li Y, Lin Q, Zhou X, Wang Q. High-throughput study of the effects of celestrol on activated fibroblast-like synoviocytes from patients with rheumatoid arthritis. *Genes (Basel).* 2017; 8:221. <https://doi.org/10.3390/genes8090221> PMID:28878153
12. Shi K, Chen X, Xie B, Yang SS, Liu D, Dai G, Chen Q. Celestrol alleviates chronic obstructive pulmonary disease by inhibiting cellular inflammation induced by cigarette smoke via the ednrb/Kng1 signaling pathway. *Front Pharmacol.* 2018; 9:1276. <https://doi.org/10.3389/fphar.2018.01276> PMID:30498444

13. Li H, Zhang YY, Huang XY, Sun YN, Jia YF, Li D. Beneficial effect of tripterine on systemic lupus erythematosus induced by active chromatin in BALB/c mice. *Eur J Pharmacol*. 2005; 512:231–37.
<https://doi.org/10.1016/j.ejphar.2005.02.030>
PMID:[15840409](https://pubmed.ncbi.nlm.nih.gov/15840409/)
14. Liu J, Lee J, Salazar Hernandez MA, Mazitschek R, Ozcan U. Treatment of obesity with celastrol. *Cell*. 2015; 161:999–1011.
<https://doi.org/10.1016/j.cell.2015.05.011>
PMID:[26000480](https://pubmed.ncbi.nlm.nih.gov/26000480/)
15. Zhang X, Xue XC, Wang Y, Cao FF, You J, Uzan G, Peng B, Zhang DH. Celastrol reverses palmitic acid-induced insulin resistance in HepG2 cells via restoring the miR-223 and GLUT4 pathway. *Can J Diabetes*. 2019; 43:165–72.
<https://doi.org/10.1016/j.ijcd.2018.07.002>
PMID:[30287053](https://pubmed.ncbi.nlm.nih.gov/30287053/)
16. Zhang Y, Geng C, Liu X, Li M, Gao M, Liu X, Fang F, Chang Y. Celastrol ameliorates liver metabolic damage caused by a high-fat diet through Sirt1. *Mol Metab*. 2016; 6:138–47.
<https://doi.org/10.1016/j.molmet.2016.11.002>
PMID:[28123944](https://pubmed.ncbi.nlm.nih.gov/28123944/)
17. Manolagas SC. From estrogen-centric to aging and oxidative stress: a revised perspective of the pathogenesis of osteoporosis. *Endocr Rev*. 2010; 31:266–300.
<https://doi.org/10.1210/er.2009-0024>
PMID:[20051526](https://pubmed.ncbi.nlm.nih.gov/20051526/)
18. Wilson C. Bone: oxidative stress and osteoporosis. *Nat Rev Endocrinol*. 2014; 10:3.
<https://doi.org/10.1038/nrendo.2013.225>
PMID:[24189509](https://pubmed.ncbi.nlm.nih.gov/24189509/)
19. Balaban RS, Nemoto S, Finkel T. Mitochondria, oxidants, and aging. *Cell*. 2005; 120:483–95.
<https://doi.org/10.1016/j.cell.2005.02.001>
PMID:[15734681](https://pubmed.ncbi.nlm.nih.gov/15734681/)
20. St-Pierre J, Drori S, Uldry M, Silvaggi JM, Rhee J, Jäger S, Handschin C, Zheng K, Lin J, Yang W, Simon DK, Bachoo R, Spiegelman BM. Suppression of reactive oxygen species and neurodegeneration by the PGC-1 transcriptional coactivators. *Cell*. 2006; 127:397–408.
<https://doi.org/10.1016/j.cell.2006.09.024>
PMID:[17055439](https://pubmed.ncbi.nlm.nih.gov/17055439/)
21. Yu B, Huo L, Liu Y, Deng P, Szymanski J, Li J, Luo X, Hong C, Lin J, Wang CY. PGC-1 α Controls Skeletal Stem Cell Fate and Bone-Fat Balance in Osteoporosis and Skeletal Aging by Inducing TAZ. *Cell Stem Cell*. 2018; 23:193–209.e5.
<https://doi.org/10.1016/j.stem.2018.06.009>
PMID:[30017591](https://pubmed.ncbi.nlm.nih.gov/30017591/)
22. Moerman EJ, Teng K, Lipschitz DA, Lecka-Czernik B. Aging activates adipogenic and suppresses osteogenic programs in mesenchymal marrow stroma/stem cells: the role of PPAR-gamma2 transcription factor and TGF-beta/BMP signaling pathways. *Aging Cell*. 2004; 3:379–89.
<https://doi.org/10.1111/j.1474-9728.2004.00127.x>
PMID:[15569355](https://pubmed.ncbi.nlm.nih.gov/15569355/)
23. Hong W, Park J, Yun W, Kang PJ, Son D, Jang J, Kim IY, You S. Inhibitory effect of celastrol on adipogenic differentiation of human adipose-derived stem cells. *Biochem Biophys Res Commun*. 2018; 507:236–41.
<https://doi.org/10.1016/j.bbrc.2018.11.014>
PMID:[30414673](https://pubmed.ncbi.nlm.nih.gov/30414673/)
24. Huang S, Tang Y, Cai X, Peng X, Liu X, Zhang L, Xiang Y, Wang D, Wang X, Pan T. Celastrol inhibits vasculogenesis by suppressing the VEGF-induced functional activity of bone marrow-derived endothelial progenitor cells. *Biochem Biophys Res Commun*. 2012; 423:467–72.
<https://doi.org/10.1016/j.bbrc.2012.05.143>
PMID:[22683631](https://pubmed.ncbi.nlm.nih.gov/22683631/)
25. Shi C, Wu J, Yan Q, Wang R, Miao D. Bone marrow ablation demonstrates that estrogen plays an important role in osteogenesis and bone turnover via an antioxidative mechanism. *Bone*. 2015; 79:94–104.
<https://doi.org/10.1016/j.bone.2015.05.034>
PMID:[26036172](https://pubmed.ncbi.nlm.nih.gov/26036172/)
26. Almeida M, Han L, Martin-Millan M, Plotkin LI, Stewart SA, Roberson PK, Kousteni S, O'Brien CA, Bellido T, Parfitt AM, Weinstein RS, Jilka RL, Manolagas SC. Skeletal involution by age-associated oxidative stress and its acceleration by loss of sex steroids. *J Biol Chem*. 2007; 282:27285–97.
<https://doi.org/10.1074/jbc.M702810200>
PMID:[17623659](https://pubmed.ncbi.nlm.nih.gov/17623659/)
27. Lee NK, Choi YG, Baik JY, Han SY, Jeong DW, Bae YS, Kim N, Lee SY. A crucial role for reactive oxygen species in RANKL-induced osteoclast differentiation. *Blood*. 2005; 106:852–59.
<https://doi.org/10.1182/blood-2004-09-3662>
PMID:[15817678](https://pubmed.ncbi.nlm.nih.gov/15817678/)
28. Finck BN, Kelly DP. PGC-1 coactivators: inducible regulators of energy metabolism in health and disease. *J Clin Invest*. 2006; 116:615–22.
<https://doi.org/10.1172/JCI27794>
PMID:[16511594](https://pubmed.ncbi.nlm.nih.gov/16511594/)
29. Fang P, He B, Yu M, Shi M, Zhu Y, Zhang Z, Bo P. Treatment with celastrol protects against obesity through suppression of galanin-induced fat intake and activation of PGC-1 α /GLUT4 axis-mediated glucose consumption. *Biochim Biophys Acta Mol Basis Dis*.

- 2019; 1865:1341–1350.
<https://doi.org/10.1016/j.bbadis.2019.02.002>
PMID:30742994
30. Guan Y, Cui ZJ, Sun B, Han LP, Li CJ, Chen LM. Celastrol attenuates oxidative stress in the skeletal muscle of diabetic rats by regulating the AMPK-PGC1 α -SIRT3 signaling pathway. *Int J Mol Med*. 2016; 37:1229–38.
<https://doi.org/10.3892/ijmm.2016.2549>
PMID:27049825
31. Lee G, Uddin MJ, Kim Y, Ko M, Yu I, Ha H. PGC-1 α , a potential therapeutic target against kidney aging. *Aging Cell*. 2019; 18:e12994.
<https://doi.org/10.1111/acer.12994>
PMID:31313501
32. Wang Y, Li C, Gu J, Chen C, Duanmu J, Miao J, Yao W, Tao J, Tu M, Xiong B, Zhao L, Liu Z. Celastrol exerts anti-inflammatory effect in liver fibrosis via activation of AMPK-SIRT3 signalling. *J Cell Mol Med*. 2020; 24:941–53.
<https://doi.org/10.1111/jcmm.14805>
PMID:31742890
33. Guo J, Wang Y, Wang N, Bai Y, Shi D. Celastrol attenuates intrahepatic cholestasis of pregnancy by inhibiting matrix metalloproteinases-2 and 9. *Ann Hepatol*. 2019; 18:40–47.
<https://doi.org/10.5604/01.3001.0012.7860>
PMID:31113607
34. Ma X, Xu L, Alberobello AT, Gavrilova O, Bagattin A, Skarulis M, Liu J, Finkel T, Mueller E. Celastrol protects against obesity and metabolic dysfunction through activation of a HSF1-PGC1 α transcriptional axis. *Cell Metab*. 2015; 22:695–708.
<https://doi.org/10.1016/j.cmet.2015.08.005>
PMID:26344102
35. Lee JH, Koo TH, Yoon H, Jung HS, Jin HZ, Lee K, Hong YS, Lee JJ. Inhibition of NF-kappa B activation through targeting I kappa B kinase by celastrol, a quinone methide triterpenoid. *Biochem Pharmacol*. 2006; 72:1311–21.
<https://doi.org/10.1016/j.bcp.2006.08.014>
PMID:16984800
36. Kim DH, Shin EK, Kim YH, Lee BW, Jun JG, Park JH, Kim JK. Suppression of inflammatory responses by celastrol, a quinone methide triterpenoid isolated from *celastrus regelii*. *Eur J Clin Invest*. 2009; 39:819–27.
<https://doi.org/10.1111/j.1365-2362.2009.02186.x>
PMID:19549173
37. Sethi G, Ahn KS, Pandey MK, Aggarwal BB. Celastrol, a novel triterpene, potentiates TNF-induced apoptosis and suppresses invasion of tumor cells by inhibiting NF-kappaB-regulated gene products and TAK1-mediated NF-kappaB activation. *Blood*. 2007; 109:2727–35.
<https://doi.org/10.1182/blood-2006-10-050807>
PMID:17110449
38. Jannuzzi AT, Kara M, Alpertunga B. Celastrol ameliorates acetaminophen-induced oxidative stress and cytotoxicity in HepG2 cells. *Hum Exp Toxicol*. 2018; 37:742–51.
<https://doi.org/10.1177/0960327117734622>
PMID:28984147
39. Su T, Xiao Y, Xiao Y, Guo Q, Li C, Huang Y, Deng Q, Wen J, Zhou F, Luo XH. Bone marrow mesenchymal stem cells-derived exosomal MiR-29b-3p regulates aging-associated insulin resistance. *ACS Nano*. 2019; 13:2450–62.
<https://doi.org/10.1021/acsnano.8b09375>
PMID:30715852
40. Li CJ, Cheng P, Liang MK, Chen YS, Lu Q, Wang JY, Xia ZY, Zhou HD, Cao X, Xie H, Liao EY, Luo XH. MicroRNA-188 regulates age-related switch between osteoblast and adipocyte differentiation. *J Clin Invest*. 2015; 125:1509–22.
<https://doi.org/10.1172/JCI77716>
PMID:25751060
41. Li CJ, Xiao Y, Yang M, Su T, Sun X, Guo Q, Huang Y, Luo XH. Long noncoding RNA *bmncr* regulates mesenchymal stem cell fate during skeletal aging. *J Clin Invest*. 2018; 128:5251–66.
<https://doi.org/10.1172/JCI99044>
PMID:30352426
42. Xie H, Cui Z, Wang L, Xia Z, Hu Y, Xian L, Li C, Xie L, Crane J, Wan M, Zhen G, Bian Q, Yu B, et al. PDGF-BB secreted by preosteoclasts induces angiogenesis during coupling with osteogenesis. *Nat Med*. 2014; 20:1270–78.
<https://doi.org/10.1038/nm.3668>
PMID:25282358